**10A.2**

# CONVECTIVE BOUNDARY LAYERS SUBJECT TO NON-STATIONARY SURFACE HEAT FLUXES

Robert van Driel and Harm J. J. Jonker*
Multi-Scale Physics, Delft University of Technology, The Netherlands

## ABSTRACT

In this study we systematically investigate the response of dry convective boundary layers to non-stationary surface heat fluxes. Not only is this relevant during sunset and sunrise, but also when for example clouds modulate incoming solar radiation. Because the timescale of the associated change in surface heat fluxes may differ from case to case, we consider in the present study the generic situation of oscillatory surface heat fluxes with different frequencies and amplitudes, and study the response of the boundary layer in terms of transfer functions. To this end we use both a Mixed Layer Model (MLM) and a Large Eddy Simulation (LES) model, where the latter is used to evaluate the predictive quality of the mixed layer model. The mixed layer model performs generally quite well for slow changes in the surface heat flux, and provides analytical understanding of the transfer characteristics of the boundary layer such as amplitude and phase-lag. For rapidly changing surface fluxes, i.e. changes within a time frame comparable to the large eddy turn-over time, it proves important to account for the time it takes for the information to travel from the surface to higher levels of the boundary layer such as the inversion zone. As a follow-up to the study of Sorbjan (1997) who showed that the conventional convective velocity scale is inadequate as scaling quantity during the decay phase, we address the issue of defining, in (generic) transitional situations, a velocity scale that is solely based on the surface heat flux and its history.

## 1. INTRODUCTION

Realistic planetary boundary layers (PBL) are often in a state of transition, adapting to changing boundary conditions or large scale forcings. Examples are sunset and sunrise, modulation of solar irradiance by clouds, and large scale advection of air with different properties. Knowledge of the behavior of transitional atmospheric boundary layers is therefore as relevant as their steady state counterparts.

The situation of decaying convective turbulence such as occurs during sunset conditions was studied by Nieuwstadt and Brost (1986) using a Large Eddy Simulation model. In this study the transition was rather abrupt as the surface heat flux was simply switched off. Pino et al. (2006) followed a similar approach and studied the influence of (steady) wind-shear during the convective decay. In addition they analysed the characteristic length-scales of the velocity fields during the decay and showed that the characteristic length scale of horizontal length scales significantly increases during the transition as opposed to the typical length-scale of the vertical velocity which remains bounded by the boundary layer depth. The increasing length-scales were shown to be responsible for the relatively slow decay already observed by Nieuwstadt and Brost (1986) ($\sim t^{-n}$ with $n$ close to 1 rather than 2). Instead of an abrupt change in the surface heat flux, Sorbjan (1997) considered the more common situation of a gradually decreasing surface flux following a cosine shape, and pointed out that during the decay the convective velocity scale based on the actual surface flux was a poor predictor of the actual velocity variances and turbulence kinetic energy. This scaling issue has also been studied based on real observations (Kumar et al., 2006) during a diurnal cycle. In addition there have been studies to the effects of a solar eclipse (Dolas et al., 2002; Girard-Ardhuin et al., 2003) and also the turbulence decay during an eclipse (Anfossi et al., 2004). Beare et al. (2006) studied the sunset transition using Large Eddy Simulation and observations. A theoretical approach was conducted by Goulart et al. (2003).

The problem of scaling during the diurnal cycle and especially the sunset phase forms the motivation of this research. We focus on the response of a convective boundary layer to changes in the surface heat flux. Not only is this relevant during sunrise and sunset, but also when for example clouds disturb the incoming solar radiation. But because the timescale of the associated change in surface heat fluxes may differ from case to case – sunrise/sunset rate for example is latitude and season dependent and blocking of sunlight can occur on various timescales– we consider in the present study the generic situation of oscillatory surface heat fluxes with different frequencies and amplitudes, and study the response of the boundary layer in terms of transfer functions.

The approach to address this issue is to first create a boundary layer which is in steady state and which subsequently gets perturbed by modifying the surface heat flux. The results are analysed by looking at the response of the mixed layer depth in terms of amplitude and phase difference. We employ both a Large Eddy Simulation (LES) model and a Mixed Layer Model (MLM), where the LES is used to evaluate the predictive quality of the mixed layer model, while the mixed layer model helps providing fundamental insight into the characteristics of the boundary layer system.

* *Corresponding author address:* Harm Jonker, Dept. of Multi-Scale Physics, Delft University of Technology, Delft, The Netherlands (h.j.j.jonker@tudelft.nl - www.msp.tudelft.nl)

## 2. CASE AND MODEL DESCRIPTION

### 2.1 *Case Description*

We consider a dry convective boundary layer in absence of mean wind and Coriolis force. The free atmosphere is stably stratified with lapse rate $\Gamma$. Turbulence is driven by a positive surface heat flux $\phi_s$, initially taken constant ($= \phi_0$), which causes a well-mixed layer that deepens by entrainment. This growth is counteracted by the presence of subsidence $w_s$ which, for simplicity, is taken constant with height, except for the lowest part of the PBL. To ensure a steady situation in the overlaying layer (free troposphere) we have also introduced a constant radiative cooling term $R$ equal to:

$$R = w_s \Gamma \tag{1}$$

The profiles of (initial) potential temperature, subsidence and radiation are shown in Fig. 1. Parameters values are listed in Table 1.

Table 1: Input parameters for the LES

| | |
|---|---|
| Domain Size $L_x \times L_y \times L_z$ | 5120×5120×1920 m$^3$ |
| Grid size $d_x \times d_y \times d_z$ | 40×40×20 m$^3$ |
| Number of gridpoints | 128×128×96 |
| Lapse rate | $\Gamma = 0.005$ K m$^{-1}$ |
| Subsidence | $w_s = 0.015$ m s$^{-1}$ |
| Surface heat flux (steady) | $\phi_0 = 0.06$ K m s$^{-1}$ |

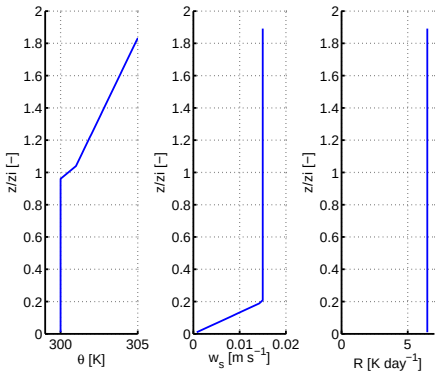


FIG. 1: The input profiles for the LES and MLM used in this research.

### 2.2 *Mixed Layer Model for stationary fluxes*

The graphical interpretation of the case within the context of a mixed layer model is shown in figure 2. Taking subsidence and radiative cooling into account, we arrive at the following equations for the mixed layer model:

$$\frac{\partial \theta}{\partial t} = \frac{\phi_s - \phi_e}{z_i} - R \tag{2}$$

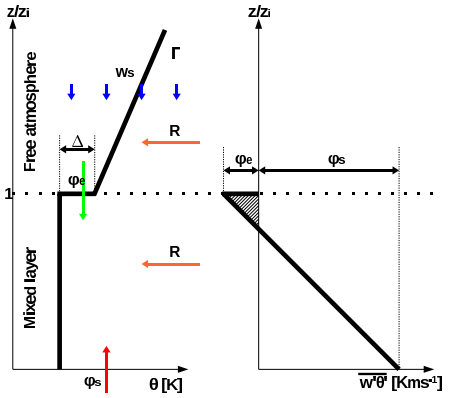


FIG. 2: The Mixed Layer Model according to this research.

$$\frac{\partial \Delta}{\partial t} = \Gamma w_e - \frac{\partial \theta}{\partial t} - R \tag{3}$$

$$\frac{\partial z_i}{\partial t} = w_e - w_s \tag{4}$$

where $\phi_e$ is the entrainment flux, $w_e$ is the entrainment velocity, $w_s$ represents subsidence and $R$ is the radiative forcing in the mixed layer and the free atmosphere. Using a zero order model (Lilly, 1968) the entrainment flux can be expressed in terms of the entrainment velocity and inversion strength $\Delta$

$$\phi_e = -w_e \Delta \tag{5}$$

To close the model the entrainment flux is assumed to be a constant fraction of the surface flux (e.g. Ball, 1960; Tennekes, 1973)

$$\phi_e = -A\phi_s \tag{6}$$

where $A$ is the entrainment ratio with a typical value of 0.2-0.3. This results in a system governed by the following equations:

$$\frac{\partial \Delta}{\partial t} = \frac{A\phi_s \Gamma}{\Delta} - \frac{(1+A)\phi_s}{z_i} = f(\Delta, z_i, \phi_s) \tag{7}$$

and

$$\frac{\partial z_i}{\partial t} = \frac{A\phi_s}{\Delta} - w_s = g(\Delta, z_i, \phi_s) \tag{8}$$

### 2.3 *Fixed points and stability in the case of a stationary heat flux*

With a uniform (i.e. height independent) subsidence profile, it is *a priori* unclear whether in general a steady state can be reached. This question can be conveniently addressed by analysing the mixed layer model equations, i.e. by finding the fixed points and classifying their stability. In addition this provides information on the inherent timescales of the system. Assuming a stationary surface heat flux $\phi_s = \phi_0$ the fixed points of the system (7,8) can be determined by setting $\frac{\partial \Delta}{\partial t} = \frac{\partial z_i}{\partial t} = 0$. This results in only one fixed point solution $(\Delta_0, z_{i0})$:

$$\begin{aligned} \Delta_0 &= \frac{A\phi_0}{w_s} \\ z_{i0} &= \frac{(1+A)\phi_0}{\Gamma w_s} \end{aligned} \tag{9}$$

We note in passing that these values together with (1) imply that also $\frac{\partial \theta}{\partial t} = 0$.

The local stability of the fixed point can be studied by perturbing it slightly:

$$\begin{array}{lll} \Delta(t) = \Delta_0 + \Delta'(t) & \text{with} & \Delta' \ll \Delta_0 \\ z_i(t) = z_{i0} + z_i'(t) & \text{with} & z_i' \ll z_{i0} \end{array} \tag{10}$$

Neglecting higher order terms of the perturbations one arrives at the following form:

$$\frac{\partial}{\partial t}\begin{pmatrix} \Delta' \\ z_i' \end{pmatrix} = J(\Delta_0, z_{i0}) \begin{pmatrix} \Delta' \\ z_i' \end{pmatrix} \tag{11}$$

where $J$ is the Jacobian

$$J = \begin{pmatrix} \frac{\partial f}{\partial \Delta} & \frac{\partial f}{\partial z_i} \\ \frac{\partial g}{\partial \Delta} & \frac{\partial g}{\partial z_i} \end{pmatrix} \tag{12}$$

and $J(\Delta_0, z_{i0})$ denotes the Jacobian in the fixed point which is given by

$$J(\Delta_0, z_{i0}) = \begin{pmatrix} -\frac{w_s^2 \Gamma}{A\phi_0} & \frac{\Gamma^2 w_s^2}{(1+A)\phi_0} \\ -\frac{w_s^2}{A\phi_0} & 0 \end{pmatrix} \tag{13}$$

The eigenvalues of the Jacobian, which reveal the stability of the fixed point, are found to be

$$\lambda_{1,2} = -\frac{1}{2}\frac{\left(1 + A \pm \sqrt{(1-3A)(1+A)}\right)\Gamma w_s^2}{A(1+A)\phi_0} \tag{14}$$

Clearly the real parts of the eigenvalues are always negative which implies that the fixed point is unconditionally stable. The eigenvalues are complex valued when $A > 1/3$ indicative of (damped) oscillatory behavior. The eigenvalues also give insight in the inherent timescales of the system. When $0 < A < 1/3$ there are two time-scales given by the negative reciprocal value of the eigenvalues

$$\tau_{\pm} = \frac{2A}{1 \pm \sqrt{(1-3A)/(1+A)}} \frac{\phi_0}{\Gamma w_s^2} \tag{15}$$

When $1/3 \leq A < 1$ the eigenvalues are complex valued and the response timescale follows from the real part

$$\tau = \frac{2A\phi_0}{\Gamma w_s^2} \tag{16}$$

### 2.4 *Fixed points and stability for the case of a non-stationary heat flux*

Similar calculations can be performed for a non-stationary surface heat flux $\phi_s(t) = \phi_0 + \phi'(t)$ when we assume that amplitude of the fluctuations are small. The fixed point of the system is the same as for the stationary case (9), but the (linearised) perturbed system now reads

$$\frac{\partial}{\partial t}\begin{pmatrix} \Delta' \\ z_i' \end{pmatrix} = J(\Delta_0, z_{i0}, \phi_0) \begin{pmatrix} \Delta' \\ z_i' \end{pmatrix} + \begin{pmatrix} \frac{\partial f}{\partial \phi_s} \\ \frac{\partial g}{\partial \phi_s} \end{pmatrix} \phi' \tag{17}$$

where $J(\Delta_0, z_{i0}, \phi_0)$ is again the Jacobian in the fixed point. The driver of the system is $\phi'$; $\Delta'$ and $z_i'$ respond to this driver. Taking

$$\begin{array}{rcl} \phi' & = & \hat{\phi} e^{i\omega t} \\ \Delta' & = & \hat{\Delta} e^{i\omega t} \\ z_i' & = & \hat{z}_i e^{i\omega t} \end{array} \tag{18}$$

the system (17) becomes

$$i\omega \begin{pmatrix} \hat{\Delta} \\ \hat{z}_i \end{pmatrix} = J(\Delta_0, z_{i0}, \phi_0) \begin{pmatrix} \hat{\Delta} \\ \hat{z}_i \end{pmatrix} - \begin{pmatrix} 0 \\ \frac{w_s}{\phi_0} \end{pmatrix} \hat{\phi} \tag{19}$$

This can be written as:

$$\begin{pmatrix} \hat{\Delta} \\ \hat{z}_i \end{pmatrix} = \{J(\Delta_0, z_{i0}, \phi_0) - i\omega I\}^{-1} \begin{pmatrix} 0 \\ \frac{w_s}{\phi_0} \end{pmatrix} \hat{\phi} \tag{20}$$

where $I$ is the unit matrix. Solving equation (20) gives the responses $\hat{\Delta}$ and $\hat{z}_i$ as a function of $\omega$

$$\hat{\Delta} = -\frac{w_s^3 \Gamma^2 A \hat{\phi}}{\phi_0^2 \omega^2 A(1+A) - \Gamma^2 w_s^4 - i\phi_0 \omega \Gamma w_s^2 (1+A)} \tag{21}$$

$$\hat{z}_i = -\frac{w_s(i\omega A\phi_0 + \Gamma w_s^2)(1+A)\hat{\phi}}{\phi_0^2 \omega^2 A(1+A) - \Gamma^2 w_s^4 - i\phi_0 \omega \Gamma w_s^2 (1+A)} \tag{22}$$

Without loss of generality we can set $\hat{\phi} = 1$. Furthermore it is convenient to express the response $\hat{z}_i$ in an amplitude $Z(\omega) = |\hat{z}_i|$ and phase difference $\Psi(\omega)$:

$$\hat{z}_i = Z(\omega) e^{i\Psi(\omega)} \tag{23}$$

We emphasize that the above expressions for the response of the mixed layer to non-stationary fluxes are derived for very small fluctuations around the basic state. Since the original system is non-linear one cannot directly generalise this behavior for larger amplitude variations. In the next section both the LES and the mixed layer model will be subjected to finite surface flux variations of the form

$$\phi_s(t) = \phi_0 + \alpha \sin(\omega t) = \phi_0 + \alpha \sin(\frac{2\pi}{T} t) \tag{24}$$

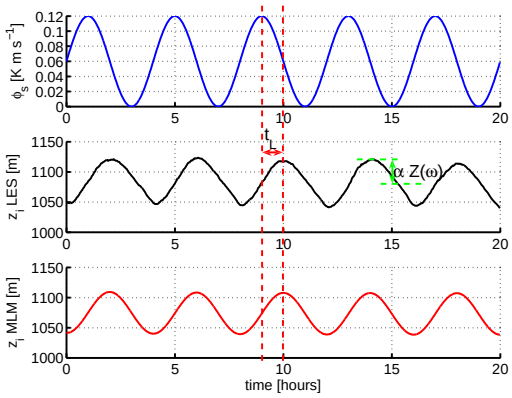


FIG. 3: Example of a non-stationary surface heat flux oscillating with a period of $T = 4$hr. Middle panel: Time series of the inversion height as simulated by the LES with an indication of the time-lag $t_L$ and amplitude of transfer $Z(\omega)$. Bottom panel: Time series of $z_i$ as resulting from the mixed layer model (7,8).

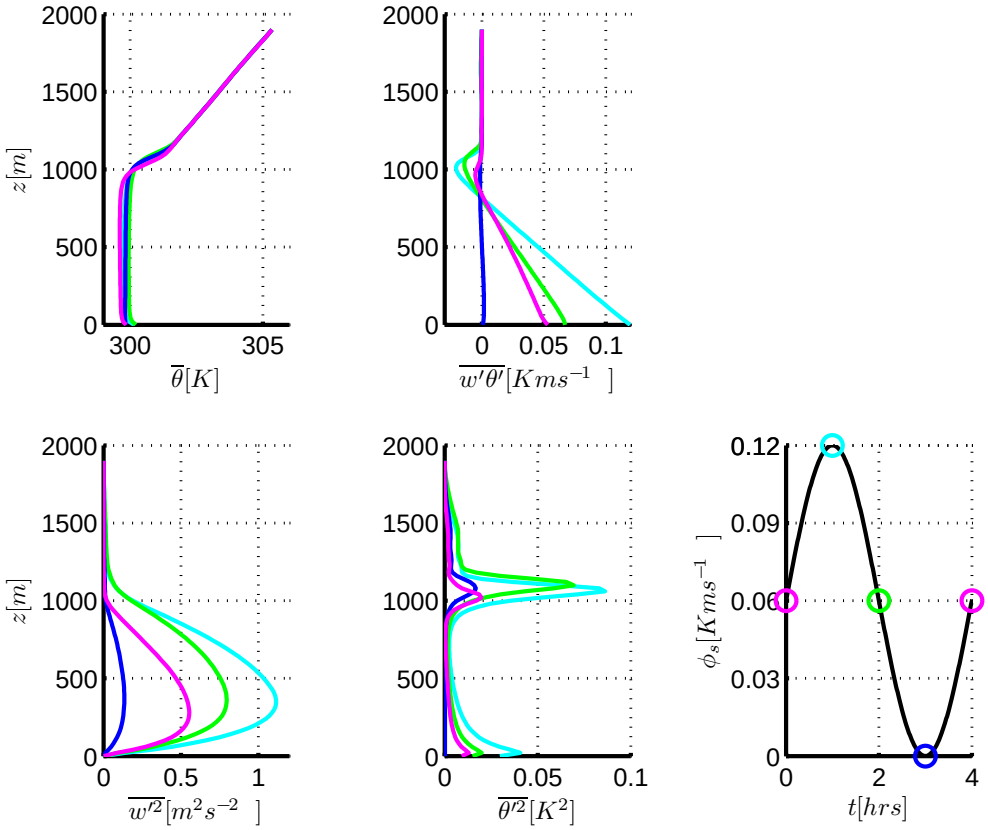


FIG. 4: The results of phase averaged of LES results with a non-stationary surface heat flux oscillating with a period of $T = 4$hr. The top two figures show the potential temperature, $\overline{\theta}$ and the buoyancy flux, $\overline{w'\theta'}$. The bottom figures shown the moments, $\overline{w'^2}$ and $\overline{\theta'^2}$ and the surface heat flux,$\phi_s$.

where $\alpha$ is the amplitude and $\omega$ is the frequency of the surface heat flux, $T$ is the period of the surface heat flux and $\phi_0$ is the average surface heat flux. $\alpha$ will be taken as large as $\phi_0$. The resulting response of the PBL will be compared to the predictions of the linearized response (22).

## 3. RESULTS

### 3.1 *LES and standard Mixed Layer Model*

Figure 3 shows an example of a periodically oscillating heat flux using (24) with $\alpha = \phi_0$ and period $T = 4$hr; below we have shown the evolution of $z_i$ as simulated with the LES, where $z_i$ was determined by location the maximum gradient in the mean profile of $\theta$ (Sullivan et al., 1998). One can notice a significant delay $t_L \simeq 1$hr between $z_i$ and $\phi_s$, which expressed in terms of the phase difference $\Psi$ reads:

$$t_L = \frac{\Psi T}{2\pi} \tag{25}$$

We will study the phase lag as well as amplitude of the response in more detail below, but first we show the mean profiles of the LES at different stages in figure 4. The periodicity in the LES response enables us to compute so-called phase averaged profiles of mean properties, fluxes and variances. The benefit of phase averaging is that a large number of samples can be collected by running the simulation for a very long time, i.e. over many periods, while conditioning the averages with respect to phase. This greatly aids the statistical quality of the averages.

Based on the heat flux profile we have estimated the value of the entrainment ratio $A$, which we determined by extrapolating the linear part of the flux observed at $z < 2z_i/3$ to the inversion height $z_i$. A value of $A \simeq 0.34$ was found in this way and was used in the mixed layer model. The response of the mixed layer model is also shown in Fig. 3. Clearly for this setting the mixed layer model is very well capable of predicting the PBL depth for an oscillating surface heat flux.

To get information on the PBL response for other driving frequencies $\omega = 2\pi/T$ and amplitudes $\alpha$, we have conducted a comprehensive study to the corresponding amplitudes $Z(\omega)$ and phase differences $\Psi(\omega)$. Results of the LES are presented in Figures 5(a) and 5(b) together with the predictions (22,23) based on the *linearized* version of the mixed layer model. One notices that the predictions of the response work quite well for slow changes,

i.e. $\omega < 10^{-4}\text{s}^{-1}$ or $T$ larger than $\approx 17.5$hr. This is interesting because the predictions appear to work well even for large amplitudes $\alpha$, hence well outside the intended working range of small amplitudes $\alpha \ll \phi_0$. Apparently for slow changes the response of the essentially non-linear mixed layer model (7,8), can be well approximated by the linearized version of the model around the stationary state $(\Delta_0, z_0)$ given by (9). Recall that this fixed-point follows from the non-linear model. A second rather striking aspect is the appreciable phase difference for small $\omega$. Even at $\omega = 10^{-5}\text{s}^{-1}$ ($T \simeq 175$hr) the phase difference is about $\pi/4$, corresponding to a time-lag of $t_L \approx 22$hr. Apparently the internal time scale of the boundary layer system is quite large. Mathematically this can be understood from the analysis of the eigenvalues of the system's Jacobian (14) and related timescale(s) (15) or (16), which is proportional to $2A\phi_0/(\Gamma w_s^2) \approx 10$hr. Physically this large time-scale can be understood by realizing that the $(z_i, \Delta)$–dynamics is governed by the entrainment velocity, leading to a time-scale estimate of $z_i/w_e$. Steady state considerations give $w_e = w_s$ and $z_{i0} = \phi_0/(\Gamma w_s)$, which

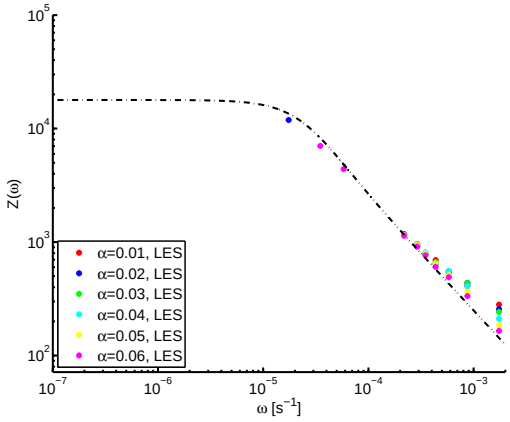


(a) **Transfer function of the standard MLM.**

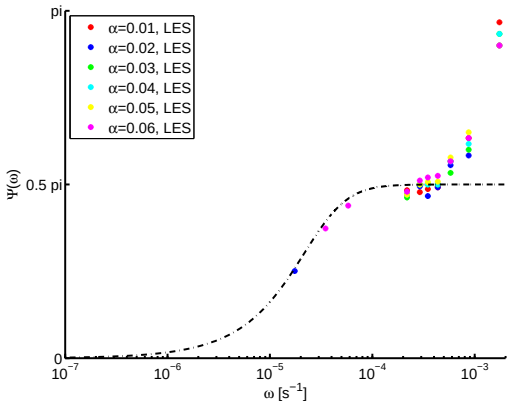


(b) **Phase difference of the standard MLM.**

FIG. 5: In these figures the analytical (linearised) solution of the standard mixed layer model (dashed lines) and the results with different amplitudes of the LES (symbols) are shown.

leads to $t_L \sim \phi_0/(\Gamma w_s^2)$. Both $w_s$ and $\Gamma$ may differ somewhat from the values we have used here, but not much, since the order of magnitude of subsidence $w_s$ is cm s$^{-1}$, $\Gamma$ is typically a few K km$^{-1}$ and surface fluxes are in the range of $0.01$–$0.1$K m s$^{-1}$. This implies that the dynamics that governs $z_i$ and $\Delta$ is much slower than the timescale of turbulence ($\simeq$15min) and even quite slow with respect to the time-scale of the diurnal cycle itself. This in turn implies that the system will always be in a transient state, hardly adapted the new conditions set by sunrise, sunset, or changed large-scale forcings.

Returning to Figures 5(a) and 5(b) once notices a discrepancy between the MLM-predictions and the LES results for fast changes, most clearly seen at the phase-differences of the LES that tend to $\pi$, whereas the MLM has a maximum phase difference of $\pi/2$. This is a natural consequence of the fact that the mixed layer model assumes instantaneous mixing, while in reality (and LES) the mixing is governed by the time-scales of turbulence. When the surface heat flux changes at a rate comparable to the time-scale of turbulence the situation becomes more intricate. This issue is addressed in the next section.

### 3.2 *rapidly changing surface fluxes*

For stationary surface heat fluxes the vertical velocity variance, $\left\langle \overline{(w')^2} \right\rangle$, can be well predicted (scaled) by the Deardorff (e.g. Sullivan et al., 1998) convective velocity scale:

$$w_{DD}^* = \left[ \frac{g z_i(t)}{\Theta_0} \phi_s(t) \right]^{\frac{1}{3}} \tag{26}$$

However for non-stationary surface heat fluxes the performance of (26) is not ideal (Sorbjan, 1997). This aspect is shown in Figure 6. When there is a good correlation (as to be expected for a scaling quantity), the points would lie on a line; for slowly changing fluxes ($T = 8$hr) this appears to be the case; however, for more rapidly changing fluxes the graphs obtain a circular shape indicative of the

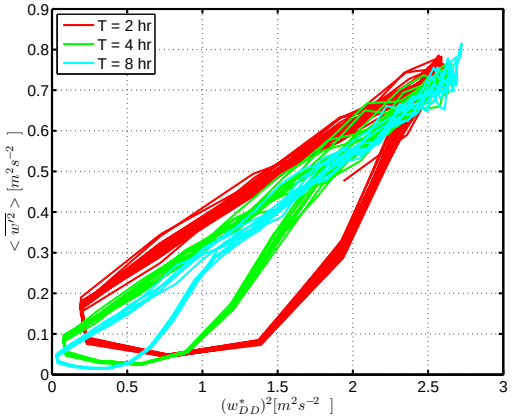


FIG. 6: A Lissajous diagram of $(w_{DD}^*)^2$, convective velocity and $\left\langle \overline{(w')^2} \right\rangle$.

phase difference between the actual variance and the actual surface flux $\phi_s$.

In order to improve the predictions of the mixed layer model for rapidly changing surface fluxes and to come up with a better prediction of the turbulence kinetic energy (tke) levels and velocity variances, we expand the mixed layer model with an extra equation that accounts for production and dissipation:

$$\frac{\partial k(t)}{\partial t} = P(t) - C_\varepsilon \frac{k(t)^{3/2}}{z_i} \tag{27}$$

where $C_\varepsilon$ is a constant and where $k$ and $P$ represent mixed layer averages of tke and buoyancy production respectively. The production term in this equation is modeled by:

$$P(t) = \frac{1}{z_i} \int_0^{z_i} \widetilde{P}(z,t) \mathrm{d}z \tag{28}$$

with

$$\widetilde{P}(z,t) = \frac{g}{\Theta_0} \left[ 1 - (1+A)\frac{z}{z_i} \right] \phi_s \left( t - \chi \frac{z}{\sqrt{k}} \right) \tag{29}$$

In this equation the essential aspect resides in the term $-\chi z/\sqrt{k}$ which accounts for the time it takes for information to travel from the surface to height $z$, where we have assumed that the corresponding speed scales with $\sqrt{k}$. When the turbulence level is high, information travels fast, but when $k$ is low it will take much longer before higher levels can feel the changed surface properties. $\chi$ is a constant that can be chosen freely (once). The effect of having the time delay in equation (29) is that the vertical profiles of the production can depart from the (quasi-steady) linear form and potentially yield the S-shaped curves such as observed in LES (Sorbjan, 1997). The curves following from (29) at various instances are shown in figure 7. The constant $\chi$ in equation (29) was determined by comparing the production calculated by LES with the production calculated by equation (28). In this case we determined $\chi = 0.92$. The effect of having $\chi$ in equation (28) is shown in Figure 8. There is a nice correlation between the results from LES and the modelled production. For periodic functions $\phi_s$ the integral in (28) can still be analytically solved. Now that there is a reasonable model

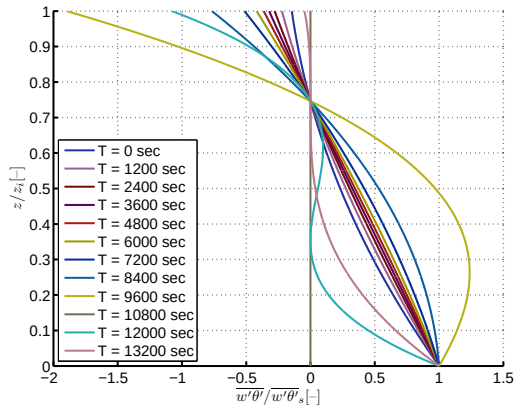


FIG. 7: Scaled $\overline{w'\theta'}$ for a surface heat flux period of 4 hours, following equation (29) with $\chi = 0.92$. The effect of the time delay provides the S-shaped curves.

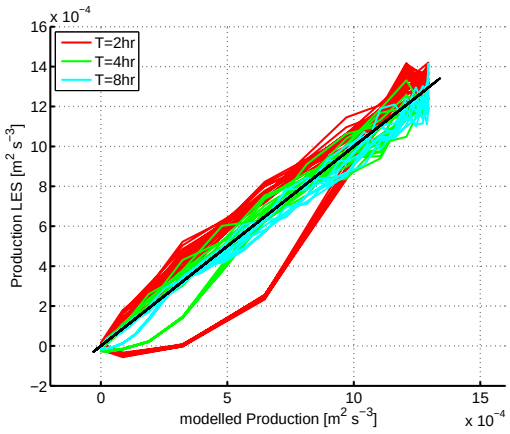


(a) **Model with $\chi = 0$ versus LES.**

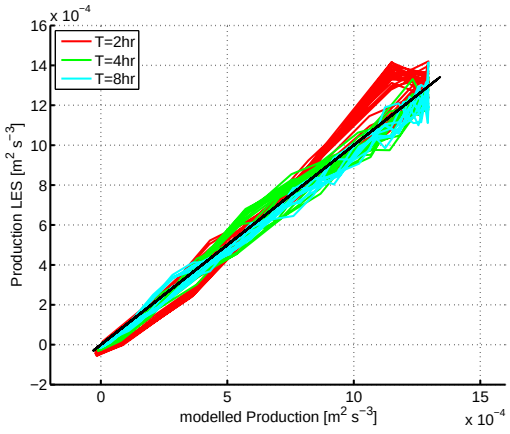


(b) **Model with $\chi = 0.92$ versus LES.**

FIG. 8: The effect of $\chi$ in the production equation with respect to the production of the LES results.

for the time-dependent buoyancy production, (27) can be solved once the constant $C_\varepsilon$ has been determined. This is done by looking at the stationary state of equation (27), i.e.

$$C_\varepsilon = \frac{P_0 z_{i0}}{k_0^{3/2}} \tag{30}$$

where $_0$ refers to the stationary state of the variable. Using LES values this resulted in a value of $1.921$ for $C_\varepsilon$. Now equation (27) can be solved, in conjunction with the other mixed layer model equations. The result of the extended MLM is shown in Figure 9 with respect to the turbulence kinetic energy calculated using LES. The correlation between the LES results and equation (27) appears to be quite good. In Figure 10 the result is shown with respect to the vertical velocity variance calculated using LES, which should be compared to Figure 6. This result shows that also for rapidly changing surface fluxes the ve-

locity variances can be anticipated using still a simple set of equations.

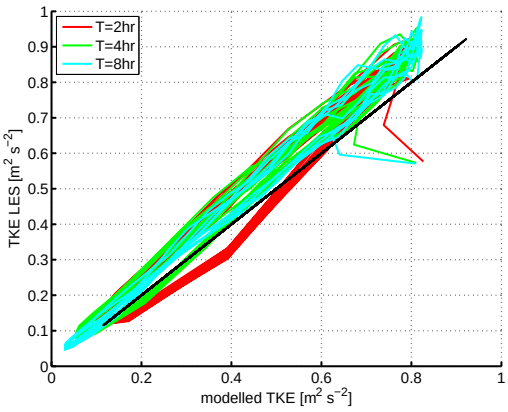


FIG. 9: The turbulence kinetic energy calculated using equation (27) with respect to the turbulence kinetic energy calculated by LES.

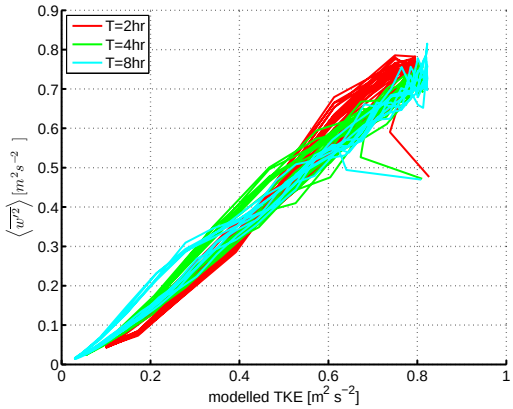


FIG. 10: The turbulence kinetic energy calculated using equation (27) versus $\left\langle \overline{(w')^2} \right\rangle$.

Since it is possible to accurately model the turbulence kinetic energy, we also used the prognostic value of $k$ in the parametrisation of the entrainment velocity. This parametrisation starts with the usual equation for the entrainment velocity

$$\frac{w_e}{w_*} = \frac{A}{\mathrm{Ri}} \tag{31}$$

where Ri is the Richardson number given by:

$$\mathrm{Ri} = \frac{\frac{g}{\Theta_0}\Delta z_i}{w_*^2} \tag{32}$$

Rearranging these equations we have for the entrainment velocity:

$$w_e = \frac{A w_*^3}{\frac{g}{\Theta_0} z_i \Delta} \tag{33}$$

The term $w_*^3$ represents the scaling velocity and should thus be replaced by $(\gamma k)^{3/2}$ where $k$ is computed from (27). The constant $\gamma$ can be calculated by comparing the scaling in steady state, which resulted in $\gamma = 3.33$.

To summarise this method the following equations are solved in the extended mixed layer model:

$$\frac{\partial \Delta(t)}{\partial t} = \Gamma w_e - \frac{\phi_s + \Delta w_e}{z_i} \tag{34}$$

$$\frac{\partial z_i(t)}{\partial t} = w_e - w_s \tag{35}$$

$$\frac{\partial k(t)}{\partial t} = P(t) - C_\varepsilon \frac{k^{3/2}}{z_i} \tag{36}$$

$$P(t) = \frac{g}{\Theta_0}\frac{1}{z_i}\int_0^{z_i}\left(1-(1+A)\frac{z}{z_i}\right)\phi_s\left(t-\chi\frac{z}{\sqrt{k}}\right)\mathrm{d}z \tag{37}$$

$$w_e = \frac{A(\gamma k)^{3/2}}{\frac{g}{\Theta_0} z_i \Delta} \tag{38}$$

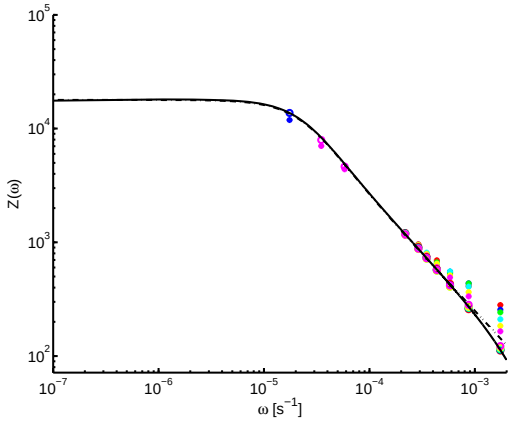


(a) **Transfer function of the new model.**

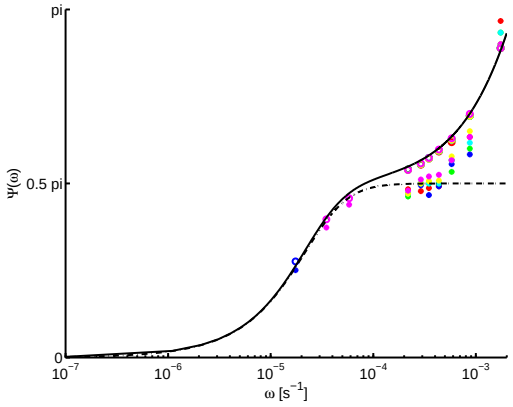


(b) **Phase difference of the new model.**

FIG. 11: In these figures the analytical (linearised) solution of the extended MLM (solid lines) the solution of the new model with different amplitudes (open symbols) the result of the standard MLM (dashed lines) and the results with different amplitudes of the LES (symbols) are shown.

The result of the extended MLM is shown again in transfer function and phase difference. These are shown

in Figures 11(a) and 11(b). The main difference between the result of the standard MLM and the extended MLM becomes clear in phase difference figure. The results of the extended MLM give comparable results as the LES result, ie. going to a phase difference of $\pi$ for high frequencies.

Also a more exotic surface heat flux was tested. The surface heat flux implemented is a square wave and is given by equation (39). The sudden jump in surface heat flux can be compared with a total solar eclipse or the modulation of the incoming solar radiation by a cloud.

$$\phi_s(t) = 0.001 + (0.12 - 0.001)\ \mathsf{H}\ (\frac{t}{T} \mathsf{mod}\ 1 - \frac{1}{2}) \quad (39)$$

where H is the Heaviside function, $T$ is the period of the square wave, in this case the period is 4 hours.

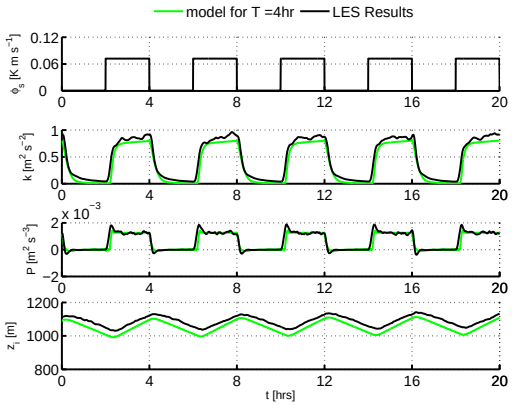


FIG. 12: The results of the extended MLM compared to the LES results with a square wave as input. The top graph shows the surface heat flux. The next figure are the results of the turbulence kinetic energy. The third graph are the results of the production. In bottom graph the results of the inversion height.

The results of this surface heat flux are shown in Figure 12. Again the extended MLM is able to reproduce the turbulence kinetic energy and the production with remarkable similarity. The inversion height is a bit lower than in the LES, but it is in phase and has the same amplitude as the LES results.

## 4. DISCUSSION AND CONCLUSION

*The standard MLM works well for slowly changing surface fluxes.* When the surface fluxes change with small frequencies or large periods, i.e. $\omega < 10^{-4}\mathrm{s}^{-1}$ or $T$ larger than $\approx 17.5$hr, the standard MLM gives quite good predictions. Both the transfer function and the phase difference are comparable to the LES results. However for rapidly changing surface fluxes the standard MLM is not able to give the right predictions.

*The non-linear mixed layer model can be very well approximated by the linearized version of the model.* This is remarkable, because the flux perturbations are well outside the range of small amplitudes, $\alpha \ll \phi_0$. Apparently the response for slow changes of the essentially nonlinear mixed layer model, can be approximated by the linearized version of the model around its stationary state, $(\Delta_0, z_{i0})$.

*Very large timescales dominate the* $(\Delta,\ z_i)$*–dynamics.* The timescales range from a few hours until a day and sometimes more. This is surprising, because usually the timescale $t^*$ is used, which is roughly 15 minutes. For the phase difference between the surface heat flux and the inversion height, this timescale is even bigger. When implementing a slowly changing surface heat flux the inversion height always responds with a delay to the surface heat flux. Only for extremely slowly varying surface heat fluxes there is a vanishing delay.

*The extended MLM works for slowly and rapidly changing surface fluxes.* When the standard MLM is expanded with the equations for the turbulence kinetic energy and the buoyancy production the model is also able to give good predictions for rapidly changing surface fluxes. When changing the surface flux very fast, i.e. a square wave, the extended MLM is able to predict the turbulence kinetic energy and the production comparable to the LES results.

## ACKNOWLEDGMENTS

This work was sponsored by the National Computing Facilities Foundation (NCF) for the use of supercomputer facilities, with financial support of NWO.

## REFERENCES

Anfossi, D., G. Schayes, G. D. Grazia, and A. Goulart, 2004: Atmospheric turbulence decay during the solar total eclipse of 11 August 1999. *Boundary-Layer Meteorology*, **111**, 301–311.

Ball, F., 1960: Control of the inversion height by surface heating. *Quarterly Journal of the Royal Meteorological Society*, **86**, 483–494.

Beare, R., J. Edwards, and A. Lapworth, 2006: Simulation of the observed evening transition and nocturnal boundary layers: Large-eddy simulation. *Quarterly Journal of the Royal Meteorological Society*, **132**, 81–99.

Dolas, P., R. Ramchandran, K. S. Gupta, S. Patil, and P. Jadhav, 2002: Atmospheric surface-layer processes during the total solar eclipse of 11 August 1999. *Boundary-Layer Meteorology*, **104**, 445–461.

Girard-Ardhuin, F., B. Bénech, B. Campistron, J. Dessens, and S. Jacoby-Koaly, 2003: Remote sensing and surface observations of the response of the atmospheric boundary layer to a solar eclipse. *Boundary-Layer Meteorology*, **106**, 93–115.

Goulart, A., G. Degrazia, U. Rizza, and D. Anfossi, 2003: A theoretical model for the study of convective turbulence decay and comparison with large-eddy simula-

tion data. *Boundary-Layer Meteorology*, **107 (1)**, 143–155.

Kumar, V., J. Keissl, C. Meneveau, and M. Parlange, 2006: Large-eddy simulation of a diurnal cycle of the atmospheric boundary layer: Atmospheric stability and scaling issues. *Water Resources Research*, **42**.

Lilly, D., 1968: Models of cloud-topped mixed layers under a strong inversion. *Quarterly Journal of the Royal Meteorological Society*, **94**, 292–309.

Nieuwstadt, F. and R. Brost, 1986: The decay of convective turbulence. *Journal of the Atmospheric Sciences*, **43 (6)**, 532–546.

Pino, D., H. Jonker, J. V.-G. de Arellano, and A. Dosio, 2006: Role of shear and the inversion strength during sunset turbulence over land: characteristic length scale. *Boundary-Layer Meteorology*, **121 (3)**, 537–556.

Sorbjan, Z., 1997: Decay of convective turbulence revisited. *Boundary-Layer Meteorology*, **82 (3)**, 501–515.

Sullivan, P., C.-H. Moeng, B. Stevens, D. Lenschow, and S. Mayor, 1998: Structure of the entrainment zone capping he convective atmospheric boundary layer. *Journal of Atmospheric Sciences*, **55 (19)**, 3042–3064.

Tennekes, H., 1973: A model for the dynamics of the inversion above a convective boundary layer. *Journal of the Atmospheric Sciences*, **30 (4)**, 558–566.